Structural and optical analysis of β-$FeSi_2$ thin layers prepared by ion-beam synthesis and solid-state reaction

V. Darakchieva, M. Baleva, and M. Surtchev
Sofia University, Faculty of Physics, 5 James Bouchier Boulevard, 1164 Sofia, Bulgaria

E. Goranova
Central Laboratory for Solar and New Energy Sources, BAS, 72 Tzarigradsko Chaussee Boulevard, Sofia 1784, Bulgaria

(Received 11 May 2000)

The β-$FeSi_2$ phase was fabricated using two different techniques: ion-beam synthesis and solid-state reaction of a thin Fe layer with Si substrate. The crystal structure of the films was investigated by grazing incident asymmetric x-ray diffraction. The generalized matrix method was used to obtain the dispersions of the absorption coefficient $\alpha(E)$ and of the refractive index $n(E)$ from the experimental transmittance and reflectance spectra, accounting for the surface and interface roughness. From $\alpha(E)$ and $n(E)$ dependences a direct band-gap energy, $E_g = 0.80$ eV was determined. When interpreting quantitatively the $\alpha(E)$ dependences, the Burstein-Moss effect was considered.

I. INTRODUCTION

Among the semiconducting silicides, β-$FeSi_2$ has attracted much attention due to its potential applications for optical sources and silicon-based optoelectronic components. Although the optical properties of β-$FeSi_2$ films have been extensively studied the nature and the value of its band gap are not unambiguously determined yet. In all optical investigations of β-$FeSi_2$ a direct band transition has been identified but there is a confusing discrepancy in the band-gap energy value—it ranges from 0.83 to 0.885 eV.[1–15] Band-structure calculations[16,17] and the experimental results on the optical absorption,[3,11,12] and the photothermal deflection spectroscopy[1,18,19] support the presence of an indirect gap of few tens of meV narrower than the direct gap. In a number of experimental works[4,12,14,15] the absorption tail or subgap absorption has been attributed to defect states within the gap. The most puzzling fact, however, is that a variety of values for the direct band gap are reported even for samples obtained by the same technique.[7]

In the present work the results on structural and optical investigations of β-$FeSi_2$ films prepared by two different techniques, ion beam synthesis (IBS) and solid state reaction (SSR) are reported. When calculating the dispersions of the optical constants of the β-$FeSi_2$ phase special attention is paid to the influence of the surface and interface roughness. The generalized matrix method used allows thorough analysis of the optical response in a wide energy region to be performed.[12,20]

II. SAMPLES PREPARATION

Two different techniques were used to fabricate iron silicide layers: IBS method: The β-$FeSi_2$ phase was formed by Fe^+ implantation into Si substrates followed by rapid thermal annealing (RTA). In order to obtain a uniform β-$FeSi_2$ layer the peak concentration of Fe^+ has to exceed the value of the stoichiometric compound ($2.6\times10^{22}\,cm^{-3}$). The concentration distribution profile of Fe^+ in a Si substrate was simulated using the TRIM program[21] in order to estimate the suitable values of energy and doses of the implanted ions. A two-step implantation process was carried out with energies E and doses D of the implanted Fe^+: $E_1 = 90$ keV, $D_1 = 4.10^{17} cm^{-2}$, and $E_2 = 25$ keV, $D_2 = 1.10^{17}\,cm^{-2}$, respectively. The second step of implantation was performed to provide a formation of comparatively thick β-$FeSi_2$ layer close to the surface. To avoid the amorphization of the substrates during the implantation they were heated to a temperature of about 400°C, by means of the incident ion beam (current density $10\,\mu A\,cm^{-2}$).[22] Subsequent to the implantation, RTA was performed in vacuum(1 Pa) to remove the residual radiation damage and to provide coalescence of the iron silicide precipitates. Two regimes of annealing of the implanted samples were used: (i) at temperature $T_a = 900$°C for 60 s (sample IS1) and (ii) at $T_a = 800$°C for 15 s with additional annealing at $T_a = 900$°C for 60 s (sample IS2).

SSR method: The sample preparation included standard Si substrates cleaning and etching prior to Fe deposition. An iron layer with a thickness of about 50 nm was then deposited on a Si substrate at room temperature in the e-beam Leybold Heraeus NT 1500 vacuum system. The formation of iron silicide resulted from the solid-state reaction between Fe layer and Si substrate during thermal annealing in argon atmosphere at $T_a = 700$°C for 15 min (sample SS50). In both preparation techniques n-type Si wafers with (100) orientation and resistivity 4.5–7.5 Ω cm were used.

III. EXPERIMENTAL RESULTS

A. GIAXRD investigations

The crystal structure of the films fabricated by IBS and SSR was investigated by grazing incident asymmetric x-ray diffraction (GIAXRD). The GIAXRD patterns were obtained by a standard x-ray diffractometer URD-6 with Cu anode and long secondary slits and a secondary plane graphite monochromator in an angular range from 20° to 60° with a

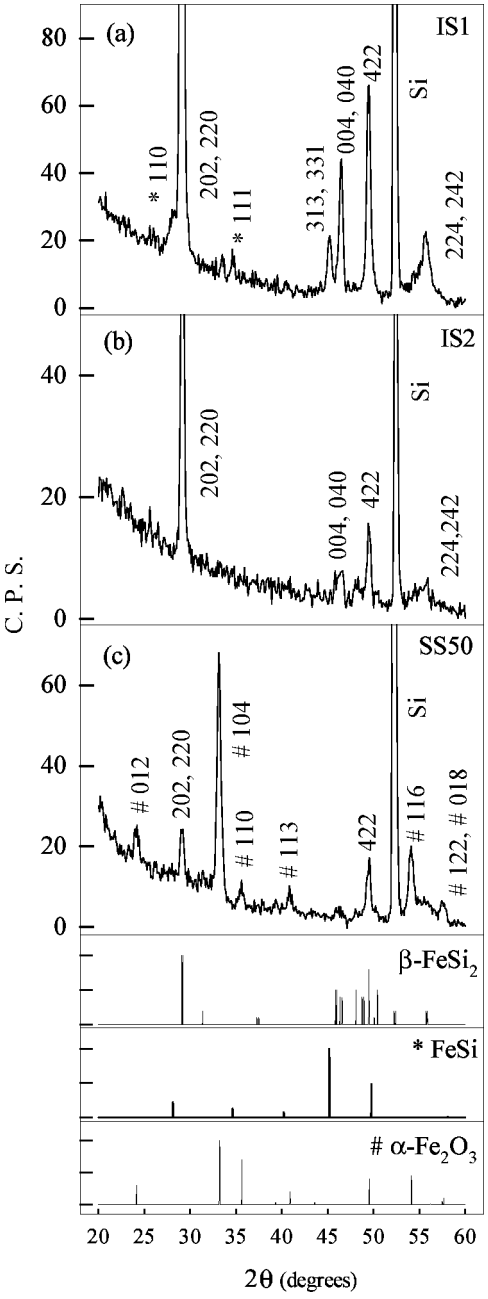

FIG. 1. Grazing incident asymmetric x-ray diffraction patterns of (a) sample IS1, (b) sample IS2, and (c) sample SS50. The diffraction patterns of polycrystal β-$FeSi_2$, FeSi and α-Fe_2O_3 with intensities and positions taken from PDF database (Ref. 23) are shown with solid lines below the experimental spectra.

step of $2\Theta = 0.05°$. The GIAXRD patterns of samples IS1, IS2, and SS50, taken at a grazing angle $\beta = 1°$ are shown in Figs. 1(a), 1(b) and 1(c), respectively. In the same figure the diffraction spectra of polycrystalline β-$FeSi_2$, FeSi, and α-Fe_2O_3 with intensities and positions taken from the powder diffraction file (PDF) database[23] are shown with solid lines below the experimental spectra.

In all three samples the β-$FeSi_2$ phase was detected. From the GIAXRD patterns the lattice parameters of the β-$FeSi_2$ phase in the samples, obtained at different technological conditions were determined. In Table I these parameters are compared with those reported for β-$FeSi_2$ thin films and bulk material,[24] and those given in the PDF database.[23] It is seen that the difference of β-$FeSi_2$ phase lattice parameters in the samples under investigation does not exceed 0.033 Å. The values of these parameters are very close to those given in PDF database[23] and reported for bulk material.[24]

TABLE I. Lattice parameters of β-$FeSi_2$ phase in samples under investigation compared with the results of other authors and PDF database.

Sample	a (Å)	b (Å)	c (Å)
IS1	9.894	7.799	7.823
IS2	9.875	7.806	7.815
SS50	9.867	7.832	7.833
β-$FeSi_2$/Si[a]	9.863	7.789	7.806
bulk β-$FeSi_2$[a]	9.881	7.805	7.834
β-$FeSi_2$/FeSi[a]	9.899	7.823	7.839
β-$FeSi_2$[b]	9.879	7.799	7.839

[a]K. Lefki *et al.* (Ref. 24).
[b]PDF database (Ref. 23).

In Table II the integral intensity ratios of the peaks detected in the patterns of the IB synthesized samples are compared with those in the standard powder-diffraction pattern.[23] It is seen that the intensity ratios of the β-$FeSi_2$ reflexes indicate a preferable growth in the (202) or (220) directions. The angular positions of the diffraction peaks (202) and (220) almost coincide, which does not allow the peaks intensity to be separately determined.

It is seen from Fig. 1(a) that in the spectrum of sample IS1 along with the β-$FeSi_2$ phase, traces of metallic FeSi are also detected. The diffraction pattern of sample IS2 [Fig. 1(b)] indicates a monophase β-$FeSi_2$ layer. However, the reflexes seen in this diffractogram are broad in comparison with those in the pattern of sample IS1. Thus, one may conclude that the samples fabricated by IBS at two stages of annealing are monophase but with less uniformity of the lattice parameters.

In the GIAXRD pattern of sample SS50 along with the well-resolved doublet (202) and (220) of β-$FeSi_2$, the reflexes of α-Fe_2O_3 are clearly seen. The high intensity of the α-Fe_2O_3 peaks in the pattern of sample SS50 might be an indication that α-Fe_2O_3 was formed mainly on the surface. To verify this assumption the sample SS50 was analyzed by GIAXRD at a grazing angle $\beta = 9°$ too. The integral intensities of β-$FeSi_2$ (220) and (202) peaks and α-Fe_2O_3 (104) peak were determined from the patterns taken at $\beta = 1°$ and $\beta = 9°$. It turned out that in the case of β-$FeSi_2$ the ratio of the intensity at $\beta = 9°$ to that at $\beta = 1°$ is 1.3, while in the case of α-Fe_2O_3 this ratio is 0.87. In other words the β-$FeSi_2$ reflexes are those hidden by the upper oxide layer.

B. Calculation of the optical constants dispersions

The room-temperature reflectance (R) and transmittance (T) spectra were measured in the range from 0.45 to 1.3 eV using CARRY-5E spectrometer. The T and R spectra of sample IS2 consisting of β-$FeSi_2$ only are shown in Fig. 2(a). In Fig. 2(b) the T spectra of sample SS50 before and after etching are compared. It is seen that after etching the T spectrum changes significantly, indicating an increased re-

TABLE II. Diffraction peak intensity ratios of β-$FeSi_2$ phase detected in IBS samples and according to PDF database.

Sample	$\frac{I_{202}+I_{220}}{I_{313}+I_{331}}$	$\frac{I_{202}+I_{220}}{I_{004}+I_{040}}$	$\frac{I_{202}+I_{220}}{I_{041}}$	$\frac{I_{202}+I_{220}}{I_{114}+I_{511}}$	$\frac{I_{202}+I_{220}}{I_{422}}$	$\frac{I_{202}+I_{220}}{I_{133}}$	$\frac{I_{202}+I_{220}}{I_{224}+I_{242}}$
IS1	17.2	12.1			6.0		12.1
IS2	12.1	13.2	12.4	15.2	5.8	17.9	
PDF data[a]	2.0	2.5	4.0	2.5	2.5	4.0	5.0

[a]PDF database (Ref. 23).

fractive index of the upper layer. The later implies that as a result of the etching the upper α-Fe_2O_3 layer ($n=2.5$) was removed to a great extent.

The optical response was analyzed in terms of a multilayered structure—air/β-$FeSi_2$/Si substrate/air. The optical constants were calculated from the experimental R and T spectra in the range of transparency of the Si substrate, from 0.45 to 1 eV, using the generalized matrix method.[20] The method allows the surface H_{sr} and interface H_{ir} roughness, as well as the effect of the finite substrate to be taken into account.

In the calculations a constant value of the refractive index of the Si substrate $n_{Si}=3.47$ was used and the imaginary part of the refractive index of the substrate k_{Si} was neglected. The film thickness was evaluated from the bulk densities of Fe, Si, and β-$FeSi_2$ and from the thickness of evaporated Fe layer and of Fe^+ implanted region of the substrate, respectively. The inversion of the experimental R and T gives no unique solutions. Therefore, in order to obtain the optical constants n and k of the β-$FeSi_2$ layer these constants were run through wide intervals, $2\leqslant n\leqslant 15$ and $0\leqslant k\leqslant 5$, so that $|R_{calc}-R_{exp}|+|T_{calc}-T_{exp}|=0$. Then the physically reasonable set of solutions consistent with the Kramers-Kronig relations was chosen.

It has been already pointed out by Bellani *et al.*[25] that the numerical inversion of R and T around the absorption edge gives numerically unstable or physically unreasonable solutions for n and k, probably due to the rough and nonideal (plane and abrupt) interfaces. The problem how to account for the interface and surface roughness is not trivial. Often physically realistic pair of solutions $n(E)$ and $k(E)$ can be found for more than one set of irregularities values. Thus, the magnitudes H_{sr} and H_{ir} cannot be included in the calculations as variable parameters. That is why, we calculated the dispersions of the optical constants with different roughness in order to estimate the uncertainty of the material characteristics involved by the roughness.

The dispersions of the absorption coefficient $\alpha(E)$ of sample IS2 calculated from the experimental R and T spectra with various values of surface and interface roughness are shown in Fig. 3. In the inset of the same figure the dispersions of the refractive index $n(E)$ of sample IS1 are presented along with the $\alpha(E)$ dependences in order to make the effect of the roughness more apparent. The calculation with finite values of the surface and interface roughness leads to the following changes in the dispersion curves: (i) The features in the spectral dependences become more pronounced. As seen from the inset in Fig. 3 the maximum in $n(E)$ dependence of sample IS1 is well defined in the curve

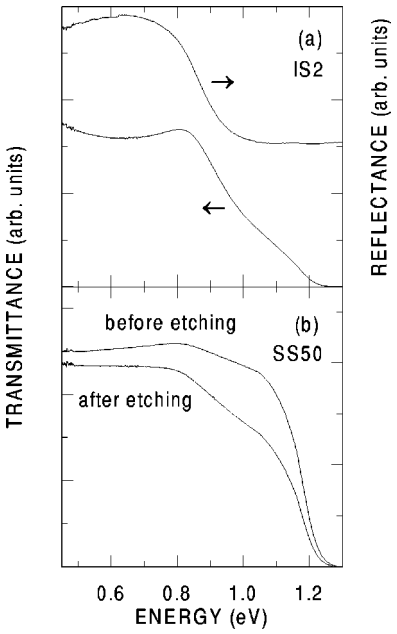

FIG. 2. Room-temperature transmittance and reflectance spectra of sample IS2 (a) and the transmittance spectra of sample SS50 before and after etching (b).

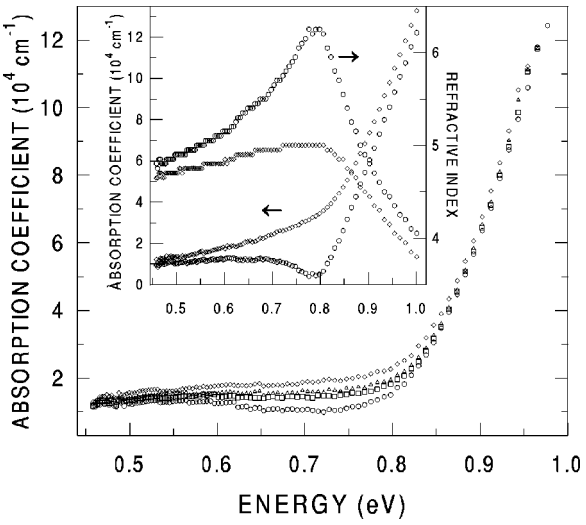

FIG. 3. Dispersions of the absorption coefficient $\alpha(E)$ of sample IS2. The inset shows the $\alpha(E)$ dependences and the refractive index dispersions $n(E)$ of sample IS1. The $\alpha(E)$ and $n(E)$ dispersions of both samples are calculated from the experimental R and T spectra using the generalized matrix method and different combinations of surface, H_{sr}, and interface, H_{ir}, roughness: $H_{sr}=0$ nm and $H_{ir}=0$ nm (rhombs); $H_{sr}=10$ nm and $H_{ir}=10$ nm (triangles); $H_{sr}=10$ nm and $H_{ir}=20$ nm (squares) and $H_{sr}=10$ nm and $H_{ir}=30$ nm (circles).

calculated with $H_{sr}=10$ nm and $H_{ir}=30$ nm. In the curve calculated with $H_{sr}=0$ nm and $H_{ir}=0$ nm, the maximum is blurred making the determination of its energy position uncertain. (ii) The values of the absorption coefficient, as expected, decrease with the increase of the irregularities heights. Thus, taking into account the roughness, the interpretation of the scattered light as an absorption can be avoided. The variation of the roughness values to $H_{sr}=10$ nm and $H_{ir}=30$ nm when calculating $\alpha(E)$ of sample IS2 leads to such a change in the low-energy part of the spectrum, so that the usual behavior for the free carriers absorption is observed below the absorption edge.

It turned out that a unique set of values of the irregularities could be found when calculating the $\alpha(E)$ and $n(E)$ dependences of the etched sample SS50. From the experimental T and R spectra of SS50, solutions for $\alpha(E)$ and $n(E)$ were found only when taking $H_{sr}=30$ nm and $H_{ir}=10$ nm.

C. Modeling of the $\alpha(E)$ dependences

The spectral dependences $\alpha(E)$ of samples IS1 and IS2, calculated with different surface and interface roughness and the unique $\alpha(E)$, dependence of sample SS50 were interpreted.

The absorption coefficient spectrum was modeled as a sum of three absorption mechanisms: fundamental absorption $\alpha_g(E)$, subgap absorption $\alpha_{sg}(E)$, and free carrier absorption $\alpha_{fc}(E)$.

1. Fundamental absorption

The values of the carrier concentration in IB synthesized undoped β-$FeSi_2$, reported so far,[1] range from 10^{18} to $10^{19}\,cm^{-3}$. At such a high carrier concentration the Fermi level is normally found in the conduction or valence band and the Burstein-Moss effect is reasonable to take place. On the other hand, the strong increase of the absorption coefficient around 0.80 eV to values of the order of $10^5\,cm^{-1}$ implies unambiguously a direct band-gap transition. In the case of Burstein-Moss effect and direct interband transition the energy dependence of the absorption coefficient, $\alpha_g(E)$, is given by

$$\alpha_g(E)=\alpha_0(E)\left[1+\exp\left(\frac{E_g+E_f-E}{\left(1+\frac{m_p}{m_n}\right)k_BT}\right)\right]^{-1}, \quad (1)$$

where m_n and m_p are the effective electron and hole masses, respectively, E_g is the gap energy, E_f is the Fermi level energy, k_B is the Boltzmann constant, and T is temperature, and

$$\alpha_0(E)=A\frac{(E-E_g)^{1/2}}{E}, \quad (2)$$

where A is a constant including fundamental constants, effective mass, and the electric dipole transition matrix element.

2. Subgap absorption

It is well known that the presence of crystal imperfections results in (i) defect levels, which at high concentration overlap spatially and broaden into a band that merges with the nearest intrinsic band (ii) localized strains, producing a deformation potential that locally alters the energy gap.[26] These effects smear the band edges and the effective gap is a superposition of locally induced gap values of various energies. According to the theoretical considerations of the absorption due to the local potential fluctuations, the absorption coefficient energy dependence has to follow the joint density of states distribution.[26] However, the experimental observations[5,26,27] show that the subgap absorption coefficient energy dependence, $\alpha_{sg}(E)$, in the case of fluctuations of any nature can be well described by the relation:

$$\alpha_{sg}(E)=\alpha(E_g)\exp\left(\frac{E-E_g}{\Delta}\right), \quad (3)$$

where Δ is a characteristic energy of the band edge broadening independent of E.

It has to be pointed out that the exponential energy dependence of the absorption coefficient may be regarded only as an interpolation of the dependences in two different regions. This dependence has no physical meaning in a wide energy range.

3. Free carrier absorption

The free carrier absorption is strongly influenced by the material microstructure. The presence of crystal imperfections leads to energy dissipation and results in high absorption in the low-energy range. As far as the samples under investigation are polycrystalline with inclusions of other phases and the absorption coefficient in the free carrier absorption range is too high, an extension of the classical Drude model was employed. A scattering from the grain boundaries and an energy-dependent damping parameter $\gamma(E)$ were assumed. The energy dependence of the parameter γ, in this case, according to Siapkas[28] can be written in the form:

$$\gamma(E)=\gamma_g+E^2\frac{V_b}{V_g}\frac{1}{\gamma_b}, \quad (4)$$

where V_b and V_g are the average volumes of the disordered grain boundary and of the grain, respectively, and γ_b and γ_g are the corresponding damping parameters.

The free carrier absorption coefficient energy dependence, $\alpha_{fc}(E)$ is given by

$$\alpha_{fc}(E)=A_2\frac{\gamma(E)}{E^2+\gamma^2(E)}, \quad (5)$$

where A_2 is a constant.

The experimental dependences $\alpha(E)$ were fitted in the whole energy range with the equation

$$\alpha(E)=\alpha_{fc}(E)+\alpha_{sg}(E)+\alpha_g(E). \quad (6)$$

In Fig. 4 the $\alpha(E)$ dependences of sample IS2 calculated from the experimental R and T with different combinations

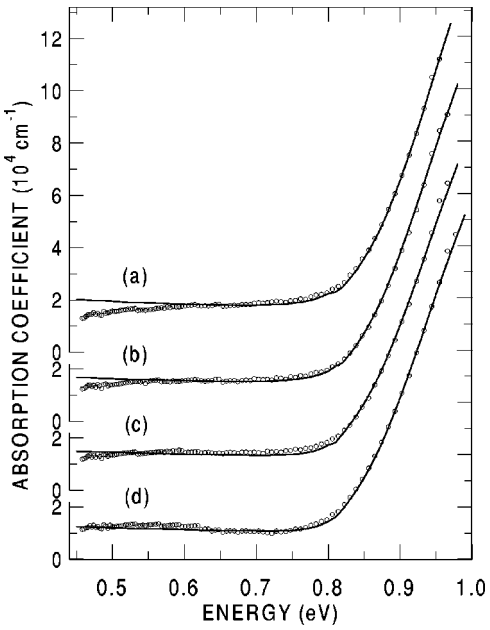

FIG. 4. Modeled (solid curves) and calculated (dots) $\alpha(E)$ spectral dependences of sample IS2 with different values of the surface H_{sr} and interface H_{ir} roughness: (a) $H_{sr}=0$ nm and $H_{ir}=0$ nm; (b) $H_{sr}=10$ nm and $H_{ir}=10$ nm; (c) $H_{sr}=10$ nm and $H_{ir}=20$ nm; (d) $H_{sr}=10$ nm and $H_{ir}=30$ nm.

of the surface and interface roughness and the dispersions of the absorption coefficient modeled with Eq. (6) are shown.

From the best fit, the quantities E_g, E_f, m_p/m_n, Δ, V_b/V_g, γ_b, and γ_g were determined. From the effective mass ratio and the Fermi level energy, the carrier concentration N was evaluated:

$$E_f=\frac{2\pi^2\hbar^2}{m_p}\left(1+\frac{m_p}{m_n}\right)\left(\frac{3N}{16\pi}\right)^{2/3}. \tag{7}$$

The effective mass of the electron $m_n=0.25\,m_0$ was taken. This value was estimated from the following equation derived from the nearly free electron band-structure approximation:

$$m_n=m_0\frac{E_g}{E_g-4E_a}, \tag{8}$$

where m_0 is the free-electron mass and

$$E_a=\frac{\hbar^2}{2m_0}\left(\frac{\pi}{a}\right)^2, \tag{9}$$

where a is the material lattice parameter.

The carrier mobilities in the grains, μ_g, and at the grain boundaries, μ_b, are evaluated from the corresponding damping parameters for each sample and combination of H_{sr} and H_{ir}. The best fit values of E_g, E_f, m_p/m_n, Δ, V_b/V_g, μ_b, and μ_g and the evaluated effective carrier mobility, μ_{eff}, are given in Table III.

IV. DISCUSSION

As seen from Table III a direct band-gap energy $E_g=0.80$ eV, independent of the roughness, is determined only for the monophase sample IS2. The variation of the irregularities does not affect strongly the value of the effective mass ratio and it remains close to 1. It has to be noticed that when accounting for the roughness Tassis *et al.*[12] has determined a direct band-gap energy of 0.80 eV for β-$FeSi_2$ thin films obtained by solid phase epitaxy and conventional vacuum furnace annealing. It is worth mentioning also that the *ab initio* band-structure calculation, performed by Christensen gives a direct gap of 0.80 eV at the Γ point of the Brillouin zone.[17] According to Christensen[17] the effective hole and electron mass values are very close to each other and the valence band maximum and the conduction band minimum states are not entirely dominated by Fe *d* states, so

TABLE III. Band gap and transport characteristics of β-$FeSi_2$ phase determined from the best fit of $\alpha(E)$ dependences, calculated with different values of the roughness.

Sample	IS1		IS2				SS50
Surface roughness H_{sr} (nm)	0	10	0	10	10	10	30
Interface roughness H_{sr} (nm)	0	30	0	10	20	30	10
Band gap energy E_g (eV)	0.75	0.80	0.80	0.80	0.80	0.80	0.80
Fermi energy E_f (eV)	0.10	0.10	0.13	0.12	0.12	0.12	0.14
Effective mass ratio m_p/m_n	2.60	1.00	1.11	1.03	1.18	1.20	1.19
Carrier concentration N x10^{-19}(cm^{-3})	7.0	4.0	5.7	5.1	5.5	5.5	6.4
Characteristic energy Δ (eV)	0.150	0.026	0.026	0.026	0.026	0.026	0.026
Fractional volume of the Disordered material V_b/V_g	0.06	0.20	0.08	0.10	0.10	0.15	0.30
Carrier mobility in the Grain μ_g(V $cm^{-2}s^{-1}$)	650	930	877	910	860	850	850
Carrier mobility at the Grain boundary μ_b(V $cm^{-2}s^{-1}$)	26	190	22	31	40	85	28
Effective carrier mobility μ_{eff} (V $cm^{-2}s^{-1}$)	3.8	53.8	3.9	6.2	8.0	21.3	10.4

that the optical transitions are not dipole forbidden. According to the theoretical calculations of Filonov[11] and Eisebitt[29] the direct gap is at Λ point and its energy value is 0.742 and 0.78 eV, respectively.

The variation of the roughness does not lead to any change of the characteristic energy Δ for the monophase sample IS2 (Table III). The value of the parameter $\Delta = 0.026$ eV is equal to k_BT at room temperature, which implies that the absorption edge tail is governed by the thermal broadening.

For the samples, where inclusions of other phases are detected (traces of FeSi phase in IS1 and α-Fe_2O_3 in SS50), the value $E_g = 0.80$ eV can be obtained only when appropriate values for the irregularities are supposed (Table III). The same band gap energy $E_g = 0.80$ eV can be unambiguously determined from the $n(E)$ dependence of sample IS1 ($H_{sr} = 10$ nm and $H_{ir} = 30$ nm), shown in the inset of Fig. 3.

The experimentally obtained values for the direct energy gap of β-$FeSi_2$, reported in the literature, are usually higher and vary from 0.83 to 0.93 eV.[1–15] The variety of values for E_g is usually attributed to a strong coupling of the band states to the lattice,[17] and thus to the particular growth conditions.[7] In our point of view the discrepancy in the gap energy value is mainly due to the variety of methods and assumptions[2,3,5,7,13–15] used to calculate the optical constants dispersions from transmittance and reflectance spectra. The discrepancy in the determination of the energy gap can be avoided if the following is taken into account:

(i) For materials available in the form of layers with a thickness of several hundred nanometers, the energy gap should be determined from the maximum of $n(E)$ dependence or from the quantitative interpretation of the dependence $\alpha(E)$. Otherwise, the strong increase of α, which takes place in these thin layers at energies higher than the energy of the edge, can be insufficiently interpreted. It has to be pointed out that at room temperature an indirect transitions absorption, if any, can be hardly detected on the background of the high subgap and free carriers absorption.

(ii) The high level of carrier concentration, when the Fermi level is placed in the band, causes a blue shift of the absorption edge. Thus, in order to determine the real energy gap value the Burstein-Moss effect has to be considered.

(iii) The roughness has to be taken into account when calculating optical constants dispersions. The latter holds to a great extent for samples with inclusions of other phases.

The values of the carrier concentration, of the order of $10^{19}\,cm^{-3}$, determined from the Fermi level energy and the effective mass are consistent with those reported for samples obtained by IBS[1] and for polycrystalline[4] and epitaxial[30] β-$FeSi_2$ layers. The effective mass values used in our calculations are approximate. However, the carrier concentration order does not change even taking several times greater effective masses.

The absorption coefficient values cannot be obtained with a great accuracy in thin films where the requirement $0.5 \leqslant \alpha d \leqslant 5$ (d is the film thickness and α is the absorption coefficient) is not fulfilled. Thus, we do not claim that the values of the carrier mobilities, evaluated from the corresponding γ parameters were determined with a great accuracy. However, one may speculate about the values of the effective carrier mobilities given in Table III, as calculated from the grain and the grain-boundary mobilities and the corresponding volumes. These values are in good agreement with the Hall mobilities reported for IB synthesized samples[1] and for polycrystalline β-$FeSi_2$ layers prepared by solid phase epitaxy.[12,31] The low values of the carrier mobility in polycrystalline films, reported so far, are usually related to a large scattering from the films imperfections.[4,32] On the other hand, according to Christensen[17] there are reasons to believe that β-$FeSi_2$ is characterized by an unusually strong electron-phonon scattering in the band-edge states. It is seen from Table III that the carrier mobilities in the grains are fairly high, suggesting a scattering mechanism from grain boundaries rather than material nature involved limitations.

V. CONCLUSIONS

On the base of the structural investigations of iron-silicide samples obtained by IBS and SSR it is found that monophase β-$FeSi_2$ layers can be formed by IBS with high doses of implantation and at two stages of RTA.

A direct gap with an energy $E_g = 0.80$ eV was determined from the $n(E)$ and $\alpha(E)$ dependences, calculated using the generalized matrix method. The $\alpha(E)$ dependences are modeled in a wide energy region as a superposition of free carrier absorption in the presence of grain boundaries, subgap absorption due to local potential fluctuations, and direct interband transitions absorption in the case of the Burstein-Moss effect. On the grounds of the optical investigations it is concluded that the discrepancy in the band-gap energy can be avoided if the surface and interface roughness, as well as the Burstein-Moss effect are accounted for.

The conclusion that the low values of the Hall carrier mobilities can be attributed rather to the presence of grain boundaries than to the material nature itself can be drawn from the speculations on the free carrier absorption behavior.

ACKNOWLEDGMENTS

The authors are indebted to Ch. Angelov and A. Djakov for the preparation of the IBS samples.

[1] K. Radermarcher, R. Carius, and S. Mantl, Nucl. Instrum. Methods Phys. Res. B **84**, 163 (1994).

[2] C.H. Olk, S.M. Yalisove, and G.L. Doll, Phys. Rev. B **52**, 1692 (1995).

[3] C. Giannini, S. Lagomarsino, F. Scarinci, and P. Castrucci, Phys. Rev. B **45**, 8822 (1992).

[4] C.A. Dimitriadis, Y.H. Werner, S. Logothetidis, M. Stutzmann, J. Weber, and N. Nesper, J. Appl. Phys. **68**, 1726 (1990).

[5] Z. Yang, K.P. Homewood, M.S. Finney, M.A. Harry, and K.J. Reeson, J. Appl. Phys. **78**, 1958 (1995).

[6] Ch. Stuhlmann, Y. Schmidt, and H. Ibach, J. Appl. Phys. **72**, 5905 (1992).

[7] M. Ožvold, V. Boháč, V. Gašparík, G. Leggieri, Š. Luby, A. Luckes, E. Majkova, and P. Mrafko, Thin Solid Films **263**, 92

(1995).
[8] L. Whang, Ch. Lin, X. Chen, Sh. Zou, L. Qin, H. Shi, W.Z. Shen, and M. Östling, Solid State Commun. **97**, 385 (1996).
[9] N. Kobayashi, H. Katsumata, H.L. Shen, M. Hasegawa, Y. Makita, H. Shibata, S. Kimura, A. Obara, S. Uekusa, and T. Hatano, Thin Solid Films **270**, 406 (1995).
[10] L. Wang, M. Östling, K. Yang, L. Qin, Ch. Lin, X. Chen, S. Zou, Y. Zheng, and Y. Qian, Phys. Rev. B **54**, R11 126 (1996).
[11] A.B. Filonov, D.B. Migas, V.L. Shaposhnikov, N.N. Dorozhkin, G.V. Petrov, V.E. Borisenko, W. Henrion, and H. Lange, J. Appl. Phys. **79**, 7708 (1996).
[12] D.H. Tassis, C.L. Mistas, T.T. Zorba, C.A. Dimitriadis, O. Valassiades, D.I. Siapkas, M. Angelakeris, P. Poulopoulos, N.K. Flevaris, and G. Kiriakidis, J. Appl. Phys. **80**, 962 (1996).
[13] V. Daraktchieva, M. Baleva, E. Goranova, and Ch. Angelov, Vacuum **58**, 415 (2000).
[14] M.C. Boast and J.E. Mahan, J. Appl. Phys. **58**, 2696 (1985); **64**, 2034 (1988).
[15] K. Lefki, P. Muret, N. Cherief, and R.C. Cinti, J. Appl. Phys. **69**, 352 (1991).
[16] L. Miglio and G. Malegori, Phys. Rev. B **52**, 1448 (1995).
[17] N.E. Christensen, Phys. Rev. B **42**, 7148 (1990).
[18] B.N.E. Rösen, D. Freundt, Ch. Dieker, D. Gerthsen, A. Rizzi, R. Carius, and H. Lüth, in *Silicides, Germanides, and their Interfaces*, edited by R. W. Fathauer *et al.*, Mater. Res. Soc. Symp. Proc. No. **320** (Material Research Society, Pittsburgh, 1994), 139.
[19] K. Radermacher, O. Skeide, R. Carius, J. Klomfass, and S. Mantl, in *Silicides, Germanides, and their Interfaces* (Ref. 18), p. 115.
[20] C.L. Mitsas and D. Siapkas, Appl. Opt. **34**, 1678 (1995).
[21] J.F. Zeigler, TRIM - 96, IBM - Research, Yorktown, New York, USA.
[22] S. Mantl, Nucl. Instrum. Methods Phys. Res. B **106**, 355 (1995).
[23] PDF database, JCPDS International Centre for Diffraction Data (1997).
[24] K. Lefki, P. Muret, E. Bustarret, N. Boutarek, R. Madar, J. Chevrier, J. Derrien, and M. Brunel, Solid State Commun. **80**, 791 (1991).
[25] V. Bellani, G. Guizzetti, F. Mirabelli, M. Ptrini, S. Lagomarsino, and H. von Känel, Solid State Commun. **96**, 751 (1995).
[26] B.I. Shklovski and A.L. Efros, in *Electronic Properties of Doped Semiconductors* (Springer, Berlin, 1984).
[27] C.H. Grein and S. John, Phys. Rev. B **39**, 1140 (1989).
[28] D. Siapkas, *Annuaire de l'Universite de Sofia Kliment Ohridski*, Faculte de Physique et Technologie des Semiconducteurs (Editions de l'Academie Bulgare des Sciences, Sofia, 1988), Vol. 78, p. 110.
[29] S. Eisebitt, J.-E. Rubensson, M. Nicodemus, T. Böske, S. Blügel, W. Eberhardt, K. Radermacher, S. Mantl, and G. Bihlmayer, Phys. Rev. B **50**, 18 330 (1994).
[30] J.L. Regolini, F. Trincat, I. Berbezier, and I. Shapira, Appl. Phys. Lett. **60**, 956 (1992).
[31] D.H. Tassis, C.A. Dimitriadis, E.K. Polychroniadis, J. Brini, and G. Kamarinos, Semicond. Sci. Technol. **14**, 967 (1999).
[32] H. Lange, Phys. Status Solidi B **201**, 37 (1997).